Gartner, J.D., Renshaw, C.E., Landis, J., and Magilligan, F.J., 2023, Impact of stream power gradients on storage of sediment and carbon on channel margins and floodplains: Geology, https://doi.org/10.1130/G50339.1

Supplemental Material

The supplemental material includes:

1. Methods on flood recurrence intervals, stream power, field surveys and sample collection, and isotopes and organics
2. Table S1. Sample site locations
3. Figure S1. Cross sections at sample sites.
4. Figure S2. Photographs of representative cross sections, Waterfall and Hewes sites.
5. Figure S3. Peak annual flow by year at Mink Brook USGS gaging station.

Supplemental Methods

Flood recurrence intervals. The flood history was determined using Log Pearson Type III analysis (England et al., 2019) of U.S. Geological Survey (USGS) gaging station 01141800 on Mink Brook. The record is continuous from 1963 to 1998. Additional peak flow measurements made in subsequent years with higher than average floods, including 2006 and 2011, were not included in the flood recurrence interval analysis. The gage has a drainage area of 12 km^2.

Stream Power. Stream power was used as a proxy for downstream sediment transport, Q_s, since **Ω** scales with Q_s (Bagnold, 1977). Stream power was calculated every ~ 10 m along Mink Brook from a 1/3 arc-second digital elevation models (DEM) with ~ 10 by 10 m grid spacing from the USGS National Map (Gesch et al., 2002). DEMs were hydrologically corrected by filling spurious depressions, and flow accumulation areas were computed for each cell along river channels following methods used by the USGS StreamStats program (Ries et al., 2017).

We used a linear relationship for Q as a function of flow accumulation area, referenced to the 2-year recurrence interval peak flow measured at the Mink Brook USGS gage. Discharge was estimated at each cell along Mink Brook by the formula $Q_i = Q_{ref} (A_i/A_{ref})$, where Q_i is discharge at the cell i, Q_{ref} is discharge at a reference cell on the same river, A_i is contributing area at cell i, and A_{ref} is contributing area at the reference cell.

Slope was calculated using a least-squares best-fit of point elevation measurements along the longitudinal profile over a distance of 500 m centered at each DEM cell along the stream. The smoothing scale is consistent with other basin-scale studies that smooth over a scale ~1/10 the square root of drainage area

(Kasprak et al., 2012). Mapped Ω gradients are approximations of in-channel sediment transport gradients (given that transport thresholds are exceeded), subject to the smoothing scale and artifacts of the resolution, accuracy, and processing of DEMs.

We focus on total stream power because we are interested in Q_s for the entire flow width. This departs from other sediment transport studies that focus on unit stream power (Ω/w, where w is stream width) because it is a close analog of shear stress (Petit et al., 2005). In this methodology, the aim is to characterize the downstream changes in stream power throughout the watershed via readily available data. As such, the actual stream power at any given location is likely different for floods with different discharges. However the downstream gradients in stream power, which are the focus of the study, would likely be consistent across a range of flows. Specifically, we make the assumption that locations with downstream increases in stream power in the 2-year RI flood are also locations with downstream increases in stream power at higher floods, up to the ~25 year RI flood. Similarly, we make the assumption that locations with downstream decreases in stream power during the 2-year RI flood are also locations with downstream decreases in stream power during higher floods, up to the ~25 year RI flood.

Field surveys and sample collection. Once stream power was determined throughout the watershed, seven sites where chosen with approximately equal stream power, with 4 sites within Ω↗ reaches at river km 3.9, 5.9, 6.1 , and 9.8, and 3 sites within Ω↘ reaches at river km 4.4, 8.3, and 13.2 (Figure 2). Adjacent sites are essentially paired, with approximately similar discharge and watershed location but different gradients in stream power. Cross sections were surveyed at each site using a total station or an autolevel, and the elevation of floods of different flood recurrence intervals was modeled using Manning's equation (n-values of 0.04 for channel and 0.08 for banks). In December, 2012, 32 soil profiles were dug along the cross sections at a range of distances from the stream channel, corresponding with increasing elevation from the low-flow water surface and, equivalently, increasing flood recurrence intervals. The soil profiles extended down to the depth of refusal (ranging from 2 to 75 cm), typically marked by cobbles, boulders, or bedrock. The profiles were sectioned in the field generally at 5 to 10 cm increments, and the dimensions of each soil section were recorded. A sample of leaf litter was also taken, if present, from a 10 by 10 cm plot at the surface of the soil profiles.

Field surveys identified locations of bedrock channels, where the stream bed was predominantly bedrock with scarce alluvium.

Isotopes and organics. The sieved soil sections and leaf litter were analyzed for $^{210}Pb_{ex}$, ^{137}Cs, and ^{7}Be in accordance with methods described in Gartner et al. (2012) and Landis et al. (2016). The soil sections (n = 124) were dried at 70 °C, sieved with a 2 mm screen, weighed, and packed tightly into 105 mL plastic containers with masses ranging from 72 to 200 g. Leaf litter samples (n = 12) were dried at 70 $^{\circ}$C, weighed, and cut with scissors to fit in containers. Samples were analyzed using Canberra Broad Energy Intrinsic High Purity Germanium (HPGE) detectors to quantify gamma ray emissions. Total ^{210}Pb, ^{137}Cs, ^{7}Be, ^{226}Ra, ^{228}Ac, and ^{238}U activities were determined from gamma ray emissions at 46.6, 662, 478, 186, 911, and 63 keV, respectively. Activities were calculated by correcting for decay since collection, sample mass, counting time, and detector and photon efficiencies. $^{210}Pb_{ex}$ was calculated by subtracting ^{226}Ra activity from total ^{210}Pb activity. We account for ^{235}U interference at 186 keV by estimating ^{238}U activity from the ^{234}Th gamma ray emissions at 63 Kev and assuming a common crustal $^{235}U/^{238}U$ activity ratio. For ^{7}Be activity, interference with ^{228}Ac at 478 keV was corrected by scaling measurements of ^{228}Ac gamma ray emission at 911 keV (Landis et al., 2012).

Detector efficiency was determined by spiking representative samples with a certified uranium ore. Attenuation for ^{210}Pb, ^{7}Be and ^{137}Cs was corrected using multi-nuclide point source as described in Landis et al. (Landis et al., 2012).

Analytical error associated with gamma counting is a function of the uncertainty inherent in both photon emission statistics and in subtracting the background emissions. The uncertainty in photon emission statistics is directly related to the total number of decays or counts (n) recorded by the detector, where $\sigma_n = \sqrt{n}$. All samples were run until they accumulated between 750 and 1250 ^{210}Pb counts. The uncertainty from background subtraction was determined using the uncertainty of a linear fit of the spectral data surrounding the measured photopeaks. ^{137}Cs activities ranged from 0.0 to 22.41 Bq kg^{-1} with an average of 3.77 Bq kg^{-1}, and analytical detection limits at the 1 σ level were calculated to range from 0.01 to 0.49 Bq kg^{-1} with an average of 0.14 Bq kg^{-1}. For $^{210}Pb_{ex}$, activities ranged from 0.0 to 271.75 Bq kg^{-1} with an average of 34.34 Bq kg^{-1}, and analytical detection limits at the 1 σ level were calculated to range from 0.61 to 8.22 Bq kg^{-1} with an average of 1.68 Bq kg^{-1}.

The activities of $^{210}Pb_{ex}$ and ^{137}Cs, measured in units of Bq kg^{-1}, were converted to inventories, in units Bq m^{-2}, based on the bulk density and dimensions of each soil section. We assumed that the vast majority of the fallout radionuclides were sorbed to organic matter and mineral particles < 2 mm in diameter, and that the fallout radionuclide activity of mineral particles > 2 mm in diameter had negligible activity and did not contribute to the overall inventories of $^{210}Pb_{ex}$ and ^{137}Cs.

The loss on ignition technique was used to determine the inventory of organic matter for each soil profile (Dean, 1974). Percent organic matter was determined by mass loss on ignition in a muffle furnace. We took ~ 10 g representative subsamples from the leaf litter samples and < 2 mm fraction of each soil section, then dried the subsamples at 110 $^{\circ}$C for > 12 hours, and burned them at 550 $^{\circ}$C for 4 hours.

Subsamples were weighed before and after each step. Percent organic matter was converted to inventory of organic matter, with units kg m^{-2}, based on the bulk density and dimensions of each soil section. As with the radionuclide methods, we assumed that mineral particles > 2 mm in diameter did not contribute to the overall organic matter inventories.

In addition to the geochemical analysis of soil pits at the channel margins and floodplains, ^{7}Be activity was analyzed from in-channel sediment samples collected in riffles from 0-2 cm depth in the bed along Mink Brook annually between 2009 and 2013. These in-stream samples were treated similarly to the soil samples— dried at 70 $^{\circ}$C, sieved with a 2 mm screen, and analyzed using HPGE detectors. However, only the ^{7}Be activity was measured (units Bq/kg), not the ^{7}Be inventory (units of Bq/m^2), because these were grab samples of surface bed material rather than quantitative soil pits.

Table S1. Sample site locations.

Site #	Site Name	Easting* (m)	Northing* (m)	D_{50} (cm)	D_{84} (cm)
1	Waterfall	726071	4842449	4.2	16.9
2	Hewes	725597	4842519	4.8	12.4
3	Bent Farm	724374	4842009	5.0	11.0
4	Firehouse	724283	4841797	5.3	10.1
5	Public Works	722793	4840847	3.5	6.0
6	Boulder Forest	721507	4840899	5.0	7.7
7	Tanzi	718813	4841066	6.7	14.0

* Coordinates based on UTM Zone 18

Supplemental Figure Captions

Figure S1. Cross sections from a Ω↗ reach (red line) and Ω↘ reach (blue line) with soil profile locations (yellow dots) and 2-year flood recurrence elevation (dashed black line).

Figure S2. Photographs of representative cross sections, a: Waterfall site and b: Hewes site. Note lack of floodplain development at Waterfall site and well-developed floodplain at Hewes site.

Figure S3. Peak annual flow by year at Mink Brook USGS gaging station.

Supplemental References

Bagnold, R. A., 1977, Bed load transport by natural rivers: Water Resources Research, v. 13, no. 2, p. 303-312.

Dean, W. E., 1974, Determination of carbonate and organic-matter in calcareous sediments and sedimentary-rocks by loss on ignition - comparison with other methods: Journal of Sedimentary Petrology, v. 44, no. 1, p. 242-248.

England, J. F. J., Cohn, T. A., Faber, B. A., Stedinger, J. R., Thomas, W. O. J., Veilleux, A. G., Kiang, J. E., and Mason, R. R. J., 2019, Guidelines for determining flood flow frequency—Bulletin 17C, U.S. Geological Survey Techniques and Methods, Volume book 4, chap. B5: Reston, VA, U.S. Geological Survey, p. 148

Gartner, J. D., Renshaw, C. E., Dade, W. B., and Magilligan, F. J., 2012, Time and depth scales of fine sediment delivery into gravel stream beds: Constraints from fallout radionuclides on fine sediment residence time and delivery: Geomorphology, v. 151, p. 39-49.

Gesch, D., Oimoen, M., Greenlee, S., Nelson, C., Steuck, M., and Tyler, D., 2002, The national elevation dataset: Photogrammetric Engineering and Remote Sensing, v. 68, no. 1, p. 5-+.

Kasprak, A., Magilligan, F. J., Nislow, K. H., and Snyder, N. P., 2012, A LIDAR-derived evaluation of watershed-scale large woody debris sources and recruitment mechanisms: Coastal Maine, USA: River Research and Applications, v. 28, no. 9, p. 1462-1476.

Landis, J. D., Renshaw, C. E., and Kaste, J. M., 2012, Measurement of Be-7 in soils and sediments by gamma spectroscopy: Chemical Geology, v. 291, p. 175-185.

-, 2016, Beryllium-7 and lead-210 chronometry of modern soil processes: The Linked Radionuclide aCcumulation model, LRC: Geochimica Et Cosmochimica Acta, v. 180, p. 109-125.

Petit, F., Gob, F., Houbrechts, G., and Assani, A. A., 2005, Critical specific stream power in gravel-bed rivers: Geomorphology, v. 69, p. 92-101.

Ries, K. G., III, Newson, J. K., Smith, M. J., Guthrie, J. D., Steeves, P. A., Haluska, T. L., Kolb, K. R., Thompson, R. F., Santoro, R. D., and Vraga, H. W., 2017, StreamStats, version 4: U.S. Geological Survey Fact Sheet, v. 2017–3046, p. 4.

Supplementary Figure 1

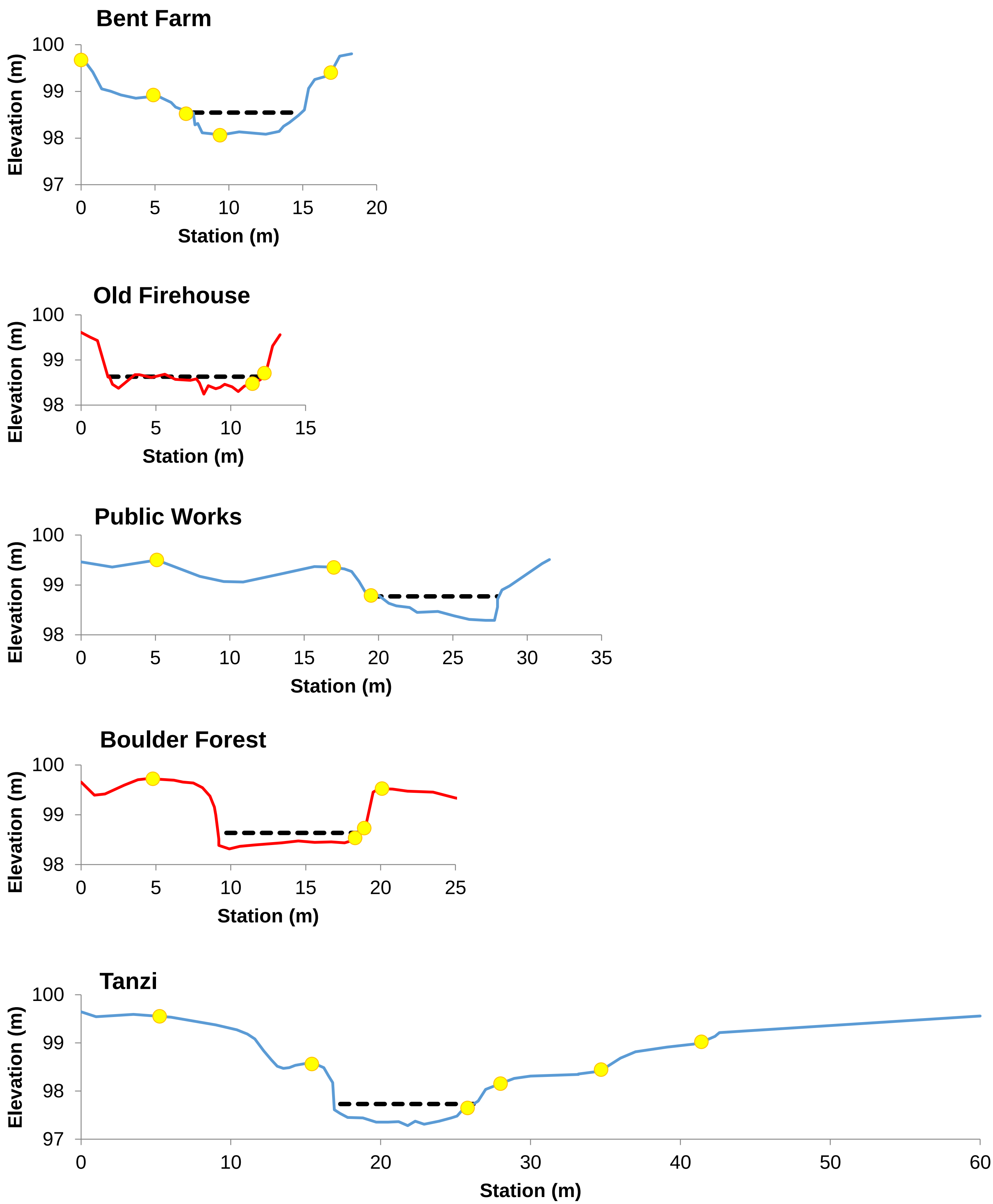

Supplementary Figure 2

Supplementary Figure 3